A Complete Si Photonics Platform Embedding Ultra-Low Loss Waveguides for O- and C-Band

Quentin Wilmart, Stephane Brision, Jean-Michel Hartmann, Andre Myko, Karen Ribaud, Camille Petit-Etienne, Laurène Youssef, Daivid Fowler, Benoit Charbonnier, Corrado Sciancalepore, et al.

Ultra-low loss silicon waveguides in a mature photonics platform

Quentin Wilmart[1], Stéphane Brision[1], Jean-Michel Hartmann[1], André Myko[1], Karen Ribaud[1], Camille Petit-Etienne[2], Laurene Youssef[2], Daivid Fowler[1], Benoit Charbonnier[1], Corrado Sciancalepore[1], Erwine Pargon[2], Stéphane Bernabé[1], Bertrand Szelag[1]

***Abstract*—We report ultra-low propagation losses in silicon sub-micrometric waveguides on a 200 mm CMOS compatible photonics platform. We show losses in C-band (O-band) as low as 0.1 dB/cm and 0.7dB/cm (0.14dB/cm and 1.1dB/cm) in monomode rib and strip waveguide geometries, respectively, thanks to a H_2 smoothing annealing. In addition to optical losses down to unprecedented levels in silicon waveguides, we show that the performance characteristics of the main passive and active building blocks of the photonics platform are preserved or even improved by the smoothing process.**

***Index Terms*— Annealing, Loss measurement, Photonic integrated circuits, Silicon photonics, Waveguide.**

I. Introduction

SILICON photonics is a prominent technology for applications as diverse as Datacom [1], [2], Lidar [3], [4], high performance computing [5] and quantum communication or computing [6], [7]. Industrial or large R&D foundries offer increasingly mature silicon photonics platforms, and have developed device libraries with stabilized device performances [8]–[11]. However, the demand is growing for increasingly complex photonic circuits, which require large numbers of components and long routing sections. Consequently, when considering the overall loss budget, it is necessary to minimize propagation losses in every device. In Datacom applications, for example, transceiver circuits typically feature centimeter-scale waveguide lengths, resulting in several dBs of propagation losses. The loss issue is even more critical in quantum photonics where ultra-low losses are required both for photon pair generation using non-linear effects [7], [12] and for single photon manipulation and routing [13].

The relatively high losses of silicon waveguides were seen for a long time as an inevitable consequence of the high optical index contrast of Si with its natural oxide cladding, the guided light being very sensitive to the waveguide roughness [14]. In return, the use of Silicon CMOS materials enable the fabrication of very dense photonic circuits. Various methods have been explored to reduce the impact of roughness on optical losses. The use of other materials e.g. SiN enables to benefit from a lower optical index and low losses [15]–[17], but this solution only works for passive circuits. Some groups have shown very good results using a high resolution immersion lithography [9], [10], [18], but the fabrication cost is substantially higher. Another route is to smooth out the sidewalls using H_2 thermal annealing. Previous studies have shown a strong reduction of Si waveguide roughness, down to sub-nanometer values [19]–[21]. Such a method showed a significant propagation loss improvement for standalone waveguides. Its implementation in a mature photonics platform including a complete set of passive and active devices was still to be demonstrated.

In this article, we demonstrate record low optical propagation losses obtained through thermal annealing. In particular, we show that its use in a mature R&D photonic platform preserves the functionalities and the performances of passive and active components of the device library. Annealed and non-annealed waveguides are compared in terms of morphological properties and propagation losses in O and C bands. The impact of the smoothing annealing on complex components such as grating fiber couplers is carefully studied. Most importantly, we also investigate the impact of annealing on the active components, and in particular, modulators based on p-n junctions.

II. Process overview

Fabrication starts using wafers with a 300nm-thick Silicon-On-Insulator (SOI) layer and 2 µm buried oxide (BOX). Three levels of silicon patterning are implemented, with an Si_3N_4 hard mask and 193nm binary photo-lithography for the first level and 248nm photo-lithography for the subsequent levels. Three types of waveguides are obtained through this process: a fully etched "strip" waveguide (300nm-thick), a partially etched "rib" waveguide with a 160nm-thick slab and a deeply etched "deep-rib" waveguide with a thin 60nm-thick slab. The latter exhibits a good trade-off between electrical access resistance and doping induced-losses in modulators. Several ion implantations steps are used before and after waveguide patterning. They are used to define p-n junctions and electrical access regions in

This work was supported by the French national program IRT Nanoelec ANR-10-AIRT-05 and the French Renatech network.

Q. W., S. B., A. M. JM. H., D. F., K. R., P. G., B. C., S. B., C. S. and B. Z. Authors are with Univ. Grenoble Alpes, CEA, LETI, F38000 Grenoble, France (e-mail: Quentin.wilmart@cea.fr).

C. PE., L. Y. and E. P. Authors are Univ. Grenoble Alpes, CNRS,LTM, 38000 Grenoble. France.

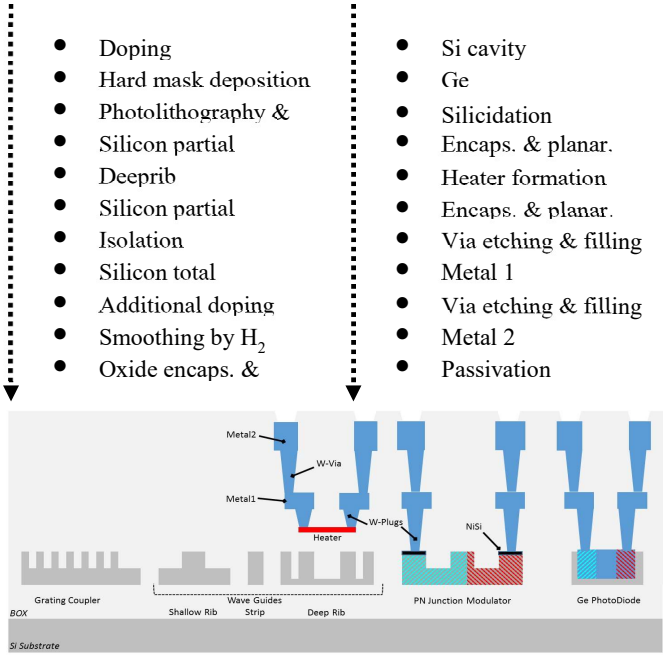

Fig. 2. Photonics platform process flow and cross section.attention le texte est coupé dans la figure Photolithography et etch, oxide encaps et planar

modulators and photodiodes. The smoothing annealing process is applied right after the waveguide patterning, prior to the encapsulation. It will be described in more detail in the next section. Photodiodes based on Germanium selective epitaxial growth inside Si cavities are fabricated [22]. The silicon contact area of active devices are defined using silicidation. Then, metallic heaters are fabricated, with 100 nm of TiN placed 600nm above the Si waveguides. A backend of line process (BEOL) is then implemented, with via contacts to the silicide and TiN and two metallization levels. A simplified process flow and the final cross section are shown in Fig. 2. We have developed a process design kit (PDK) to give access to this platform with a device library containing a large set of passive devices such as grating couplers, Multi-Mode-Interferometers, directional couplers, waveguide transitions, photodiodes and Mach-Zehnder modulators. The challenge of introducing a high-temperature smoothing process is then to preserve the performance of all these devices.

III. SILICON WAVEGUIDE SMOOTHING PROCESS

The roughness amplitude at the sidewalls of silicon waveguides can be relatively large, typically a few nanometers, after standard patterning. During H_2 thermal annealing, silicon atoms at the surface rearrange to minimize the total surface energy. This reduces the edge roughness down to sub-nanometer values with no volume change. We used a post-etching H_2 annealing process at 850°C [19]. Waveguide cross-sections with and without smoothing are shown in Fig. 1. The overall waveguide shape is preserved thanks to the presence of the Si_3N_4 hard mask on top of the waveguide. The strip waveguide (Fig. 1 a-b) has its top and bottom dimensions clamped by the Si_3N_4 hard mask

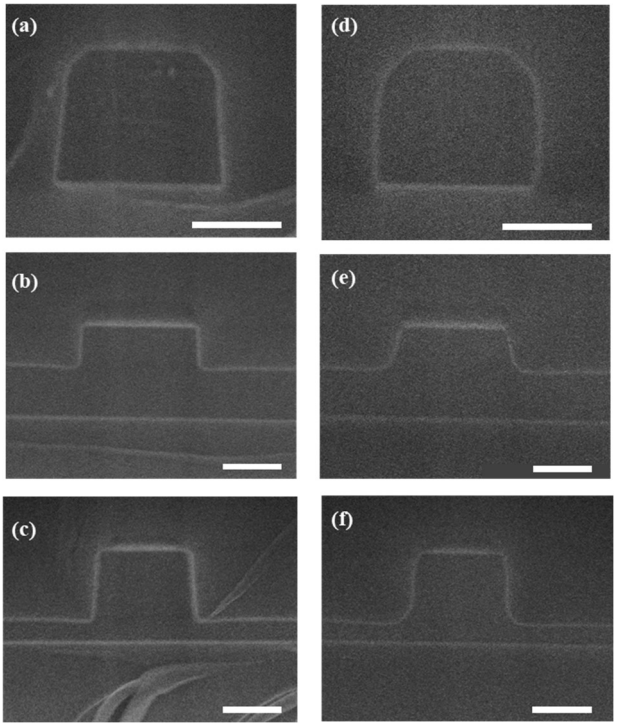

Fig. 1. SEM cross-sections of un-smoothed (a, b, and c) and smoothed (d, e and f) strip, rib and deeprib waveguides respectively. Scale: the white bar is 200nm.

and the SiO_2 substrate, respectively. We observe some corner rounding and a slight bulging of the waveguide walls. Despite these mild deformations, the annealing reduces the roughness with a limited impact on the optical mode. The rib waveguide (Fig. 1 c-d) presents a more pronounced increase of the sidewall slope. This is due to the lack of clamp at the bottom corners of the etched silicon. However, the total volume of the waveguide is preserved and the deformation remains rather small. Similarly, deep-rib waveguides show very little deformation, mainly consisting of rounded corners at the top of the waveguide and at the junction with the slab. After annealing, all structures are encapsulated with high density plasma (HDP) SiO_2.

TABLE I
PROPAGATION LOSSES

Waveguide type	No smoothing loss (σ) dB/cm	Smoothing loss (σ) dB/cm
Rib O-band	1.3 (0.12)	0.14 (0.05)
Strip O-band	3.6 (0.22)	1.1 (0.23)
Deep rib O-band	3.9 (0.23)	0.6 (0.13)
Rib C-band	0.5 (0.16)	0.1 (0.04)
Strip C-band	2.1 (0.25)	0.7 (0.17)

Median values (and standard deviation σ) of propagations losses of smoothed and unsmoothed waveguides in the O and C bands extracted from the wafer scale mappings. The waveguide widths are 350, 400 and 320nm in the O-band for rib, strip and deep rib, respectively, and 450nm and 400nm in the C-band for rib and strip waveguides, respectively.

IV. PROPAGATION LOSSES

Waveguides and devices are characterized using a semi-automatic 12 inch probe station at the wafer level with a tunable

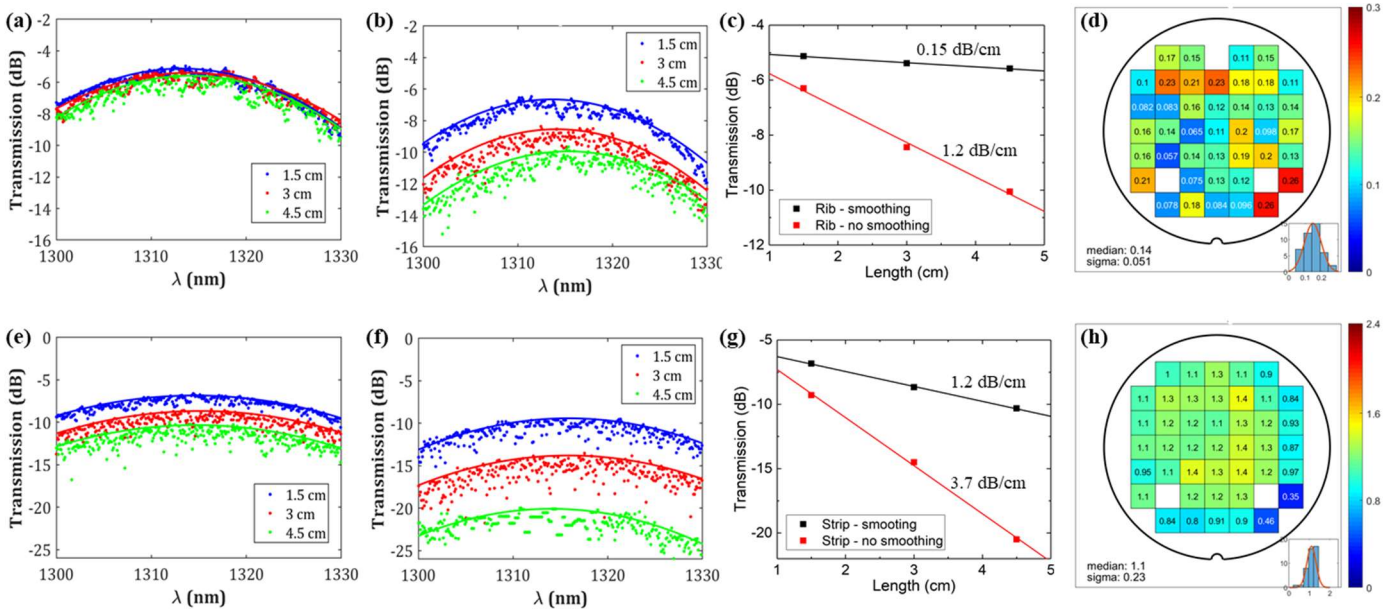

Fig. 3. O-band propagation loss measurements. (a) Raw measurement of 1.5, 3 and 4.5cm long (blue, red and green dots respectively) smoothed rib waveguides with an order 2 polynomial fit of the local maxima (solid lines). (b) Same as (a) but for unsmoothed waveguides. (c) Maximum transmission of spiraled rib waveguides as a function of their length (dots) and linear fit extracting the propagation losses of smoothed and unsmoothed rib waveguides (black and red lines, respectively). (d) Wafer scale mapping of smoothed rib waveguide propagation losses (in dB/cm). (e, f, g, and h) Same as (a, b, c, and d) but for strip waveguides.

laser source and a photodetector with pm resolution. A fiber array is used to couple the light via a surface 1D grating coupler. A single cleaved SMF28 fiber is used at the surface grating coupler output. Measurements are performed in the O-band (1300 nm) and C-band (1550 nm).

Fig. 3 shows the propagation loss measurements in the O-band using a series of spiraled waveguides 1.5, 3 and 4.5cm long with and without the smoothing process. Raw measurement data are shown for a set of rib (Fig. 3 a-b) and strip (Fig. 3 e-f) waveguides. For each measurement, the envelope (solid line) is a parabola, fitting the transmission spectrum of the grating couplers. The maximum of the fitted line defines the transmission value attributed to each structure. The waveguide propagation loss is then extracted from a linear fit (solid lines of Fig. 3 c and g) of these transmission values. Wafer level results are shown as propagation loss maps in Fig. 3 d and h for smoothed rib and strip waveguides, respectively. Statistical data (median value and standard deviation) of wafers with smoothed and unsmoothed waveguides for all types of waveguides and in the O and C bands are provided in table 1. For strip waveguides, propagation losses in the O-band are reduced from 3.6 dB/cm for the standard process down to 1.1dB/cm after the annealing process. Meanwhile, standard, non-annealed, rib waveguides show losses of 1.3 dB/cm in the O-band. The H_2 annealing reduces these propagation losses down to 0.14 dB/cm. At this point, we reach the resolution limits of the measurements, as the loss difference between the longest and the shortest spiral (3cm) is only around 0.4dB, while the experimental uncertainty is 0.3dB. Longer waveguides will be needed to accurately measure the rib propagation losses. Note also that the loss reduction is stronger in the outer ring of the wafer for strip waveguides (0.9dB/cm compared to 1.3 dB/cm, see Fig. 3 h). Even though the explanation for that is not clear (non-uniform conditions during the annealing or previous processes such as photolithography and etching) it should be therefore feasible to reduce further strip waveguide propagation losses and reach values reliably below 1dB/cm at the wafer scale. C-band results are shown in Fig. 4 (and in Table 1). Again, the propagation loss reduction is spectacular, with 0.1dB/cm (0.7dB/cm) for rib (strip) waveguides after the smoothing annealing process. Note that our C-band test structures are longer, with 2, 4 and 6 cm-long spiral waveguides.

To our knowledge, these propagation loss values are the best ever reported for single mode silicon waveguides in O and C bands [10], [23], [24] at the exception of [9] where strip waveguides patterned using immersion lithography show 0.4dB/cm loss in the C-band. The next important question is then to evaluate the impact of this annealing on more complex

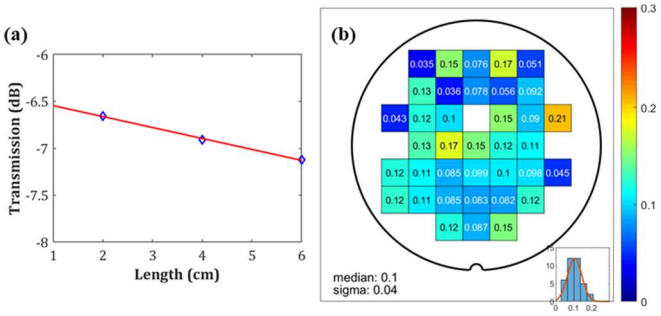

Fig. 4: C-band propagation loss measurement. (a) Maximum transmission of spiraled rib waveguides as a function of their length (blue diamond) and linear fit giving the propagation loss of the smoothed rib waveguide (red line). (b) Wafer scale mapping of smoothed rib waveguide propagation losses at 1550 nm (in dB/cm).

devices.

V. Passive Device Performance

As shown in Fig. 1 there is only a minor modification of the waveguide shape with the smoothing annealing. Accordingly, the surface grating fiber coupler performance is not impacted by the annealing step. As shown in Fig. 6, the peak transmission wavelength of annealed grating couplers is unchanged, close to the nominal value of 1310nm (1550nm) in O-band (C-band). Also, the grating fiber coupler insertion loss (~2dB) and bandwidth (~20nm at -1dB) are not impacted by the annealing.

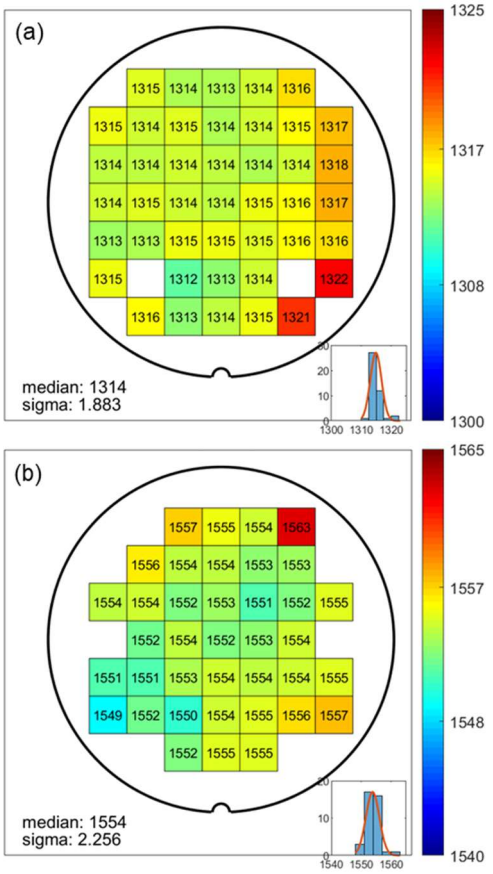

Fig. 6: Grating coupler central wavelength mapping (in nm) for (a) O-band and (b) C-band.

Bent waveguide (rib with 25µm radius) measurements even shows an improvement after annealing with bend losses going from 0.04dB/90° down to 0.02dB/90°. This improvement could be attributed to the fact that in a bent waveguide, the optical mode is slightly shifted toward the outside of the bend and therefore more sensitive to the sidewall roughness (and its reduction after annealing). Finally, we also were able to check that the smoothing annealing has no major impact on directional coupling ratios nor on MMI insertion losses.

VI. Active Devices

The Mach-Zehnder modulator (MZM) is the most common configuration of electro-optics modulator. It is based on the free carrier dispersion effect and offers fast modulation and robust fabrication [2]. The MZM is among the basic building blocks of LETI's photonics library. They are fabricated using 6 doping levels (contact, access and junction with p and n types) using the deep rib geometry. The MZM design is always a trade-off

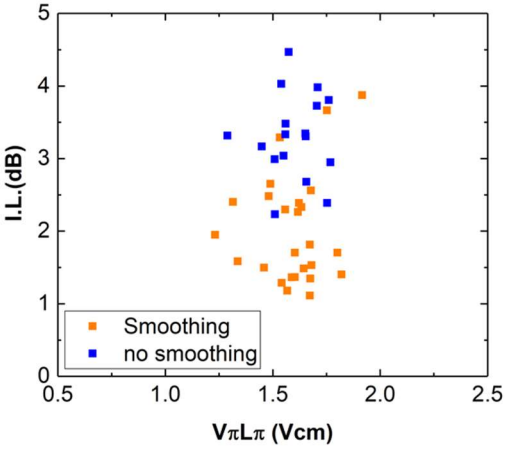

Fig. 5. Insertion loss as a function of efficiency for smoothed (orange dots) and unsmoothed (blue dots) Mach Zehnder Modulators. Data is collected from several dies of 4 different wafers. Measurement is done in the O-band.

between efficiency, optical loss and speed. Therefore, reducing the insertion loss of MZM is particularly important. Looking at the fabrication flow of Fig. 2, the p-n junction is patterned prior to the smoothing annealing, and one could argue that the relatively high temperature of the annealing step could have an impact on junction doping profile. In Fig. 5, we compare the performance of a 1mm-long MZM with and without annealing. We show the MZM efficiency versus insertion loss (de-embedded from the grating coupler loss) in several dies on two annealed and two non-annealed wafers. Fig. 5 shows a clear separation in terms of insertion loss (with a median value at 1.7dB with smoothing against 3.3dB without smoothing) while the efficiency is unchanged (the median value of $V_\pi L_\pi$ is 1.62Vcm with smoothing and 1.58Vcm without smoothing). In addition, doped waveguide propagation loss measurements show an improvement, from 8.8dB/cm without annealing to 7dB/cm with annealing. This loss reduction is directly related to the deeprib waveguide (the type of waveguide used in the active part of MZM) propagation loss improvement of Table 1. These results not only show that the smoothing annealing has no impact on the p-n junction behavior but also that it significantly reduces the insertion loss of one of the main building blocks of the photonics platform. Moreover, it provides more flexibility in terms of design tradeoffs. For instance, one could choose to increase the waveguide doping in order to reduce the driving voltage or to enhance the electrical bandwidth without an insertion loss penalty compared to previous design.

VII. Conclusion

Thanks to a H_2-based smoothing annealing, propagation losses can be considerably reduced, down to record-low levels, without compromising the performances of mature devices, nor requiring major changes in the process integration flow. The quest for loss reduction is a constant challenge in integrated

photonics and many applications rely on it. This new process is a major breakthrough for emerging applications such as quantum computation or communication.

ACKNOWLEDGMENT

This work was supported by the French national program IRT Nanoelec ANR-10-AIRT-05 and the French Renatech network

REFERENCES

[1] F. Boeuf *et al.*, « Silicon Photonics R&D and Manufacturing on 300-mm Wafer Platform », *J. Light. Technol.*, vol. 34, nº 2, p. 286-295, janv. 2016, doi: 10.1109/JLT.2015.2481602.

[2] B. Szelag *et al.*, « Multiple wavelength silicon photonic 200 mm R+D platform for 25Gb/s and above applications », présenté à SPIE Photonics Europe, Brussels, Belgium, mai 2016, p. 98911C, doi: 10.1117/12.2228744.

[3] M. J. R. Heck, « Highly integrated optical phased arrays: photonic integrated circuits for optical beam shaping and beam steering », *Nanophotonics*, vol. 6, nº 1, p. 93-107, janv. 2017, doi: 10.1515/nanoph-2015-0152.

[4] N. A. Tyler *et al.*, « SiN integrated optical phased arrays for two-dimensional beam steering at a single near-infrared wavelength », *Opt. Express*, vol. 27, nº 4, p. 5851, févr. 2019, doi: 10.1364/OE.27.005851.

[5] S. Rumley, D. Nikolova, R. Hendry, Q. Li, D. Calhoun, et K. Bergman, « Silicon Photonics for Exascale Systems », *J. Light. Technol.*, vol. 33, nº 3, p. 547-562, févr. 2015, doi: 10.1109/JLT.2014.2363947.

[6] J. W. Silverstone, D. Bonneau, J. L. O'Brien, et M. G. Thompson, « Silicon Quantum Photonics », *IEEE J. Sel. Top. Quantum Electron.*, vol. 22, nº 6, p. 390-402, nov. 2016, doi: 10.1109/JSTQE.2016.2573218.

[7] D. Grassani *et al.*, « Micrometer-scale integrated silicon source of time-energy entangled photons », *Optica*, vol. 2, nº 2, p. 88, févr. 2015, doi: 10.1364/OPTICA.2.000088.

[8] A. Rahim *et al.*, « Open-Access Silicon Photonics Platforms in Europe », *IEEE J. Sel. Top. Quantum Electron.*, vol. 25, nº 5, p. 1-18, sept. 2019, doi: 10.1109/JSTQE.2019.2915949.

[9] T. Horikawa *et al.*, « A 300-mm Silicon Photonics Platform for Large-Scale Device Integration », *IEEE J. Sel. Top. Quantum Electron.*, vol. 24, nº 4, p. 1-15, juill. 2018, doi: 10.1109/JSTQE.2018.2819893.

[10] N. M. Fahrenkopf, C. McDonough, G. L. Leake, Z. Su, E. Timurdogan, et D. D. Coolbaugh, « The AIM Photonics MPW: A Highly Accessible Cutting Edge Technology for Rapid Prototyping of Photonic Integrated Circuits », *IEEE J. Sel. Top. Quantum Electron.*, vol. 25, nº 5, p. 1-6, sept. 2019, doi: 10.1109/JSTQE.2019.2935698.

[11] R. Jones *et al.*, « Heterogeneously Integrated InP\/Silicon Photonics: Fabricating Fully Functional Transceivers », *IEEE Nanotechnol. Mag.*, vol. 13, nº 2, p. 17-26, avr. 2019, doi: 10.1109/MNANO.2019.2891369.

[12] F. A. Sabattoli *et al.*, « A Source of Heralded Single Photon Using High Quality Factor Silicon Ring Resonators », in *2019 21st International Conference on Transparent Optical Networks (ICTON)*, Angers, France, juill. 2019, p. 1-4, doi: 10.1109/ICTON.2019.8840215.

[13] N. C. Harris *et al.*, « Integrated Source of Spectrally Filtered Correlated Photons for Large-Scale Quantum Photonic Systems », *Phys. Rev. X*, vol. 4, nº 4, déc. 2014, doi: 10.1103/PhysRevX.4.041047.

[14] F. P. Payne et J. P. R. Lacey, « A theoretical analysis of scattering loss from planar optical waveguides », *Opt. Quantum Electron.*, vol. 26, nº 10, p. 977-986, oct. 1994, doi: 10.1007/BF00708339.

[15] Q. Wilmart *et al.*, « A Versatile Silicon-Silicon Nitride Photonics Platform for Enhanced Functionalities and Applications », *Appl. Sci.*, vol. 9, nº 2, p. 255, janv. 2019, doi: 10.3390/app9020255.

[16] H. El Dirani *et al.*, « Ultralow-loss tightly confining Si_3N_4 waveguides and high-Q microresonators », *Opt. Express*, vol. 27, nº 21, p. 30726, oct. 2019, doi: 10.1364/OE.27.030726.

[17] M. H. P. Pfeiffer *et al.*, « Photonic Damascene Process for Low-Loss, High-Confinement Silicon Nitride Waveguides », *IEEE J. Sel. Top. Quantum Electron.*, vol. 24, nº 4, p. 1-11, juill. 2018, doi: 10.1109/JSTQE.2018.2808258.

[18] T. Mogami, T. Horikawa, K. Kinoshita, H. Sasaki, K. Morito, et K. Kurata, « A 300mm Si photonics platform for multi-applications », in *2015 Opto-Electronics and Communications Conference (OECC)*, Shanghai, China, juin 2015, p. 1-2, doi: 10.1109/OECC.2015.7340291.

[19] C. Bellegarde *et al.*, « Improvement of Sidewall Roughness of Submicron SOI Waveguides by Hydrogen Plasma and Annealing », *IEEE Photonics Technol. Lett.*, vol. 30, nº 7, p. 591-594, avr. 2018, doi: 10.1109/LPT.2018.2791631.

[20] Q.-Q. Duan *et al.*, « Micro-Mechanism of Silicon-Based Waveguide Surface Smoothing in Hydrogen Annealing », *Chin. Phys. Lett.*, vol. 33, nº 12, p. 126801, déc. 2016, doi: 10.1088/0256-307X/33/12/126801.

[21] Q. Wilmart *et al.*, « Ultra Low-Loss Silicon Waveguides for 200 mm Photonics Platform », in *2019 IEEE 16th International Conference on Group IV Photonics (GFP)*, Singapore, Singapore, août 2019, p. 1-2, doi: 10.1109/GROUP4.2019.8925610.

[22] L. Virot *et al.*, « Integrated waveguide PIN photodiodes exploiting lateral Si/Ge/Si heterojunction », *Opt. Express*, vol. 25, nº 16, p. 19487, août 2017, doi: 10.1364/OE.25.019487.

[23] P. Absil *et al.*, « Reliable 50Gb/s silicon photonics platform for next-generation data center optical interconnects », in *2017 IEEE International Electron Devices Meeting (IEDM)*, 2017, p. 34–2.

[24] P. De Dobbelaere *et al.*, « Advanced silicon photonics technology platform leveraging a semiconductor supply chain », in *2017 IEEE International Electron Devices Meeting (IEDM)*, 2017, p. 34–1.